

Study of variable depth air pockets on air spindle vibrations in ultra-precision machine tools

M. Akhondzadeh · M. Vahdati

Received: 6 September 2013 / Accepted: 11 April 2014 / Published online: 4 May 2014
© Springer-Verlag London 2014

Abstract The low vibration of air spindle is a very important thing to achieve nanometer accuracies in the products of machined parts in nano-machining. Compared to the common air pockets with constant depth used in air cells of ultra-precision machines, this paper studied some special air pockets including five variable depth modes: flat, conical, pyramidal, spherical with two sphere radii. Considering rotational speed as well as these parameters, 18 experiments have been committed using a lathe machine. From experiment results, the air spindle with air pockets of pyramidal depth at a low rotational speed has minimum vibrations.

Keywords Ultra-precision machining · Air spindle · Variable depth · Air pocket · Vibrations

Nomenclature

a	Land width of axial flow (m)
b	Pocket depth
C	Radial clearance of bearing (m)
D	Diameter of bearing (m)
d_o	Diameter of orifice (m)
d_r	Inlet diameter
e_0	Steady-state eccentricity
F_x, F_y	Force components (N) due to air film in the x and y directions
h, \bar{h}	Film thickness (m), $\bar{h} = h/c$
L	Axial length of bearing (m)

L	Supply orifice length (m)
O_b, O_j	Bearing center, spindle, or journal center
\bar{P}	Non-dimensional pressure
P_a	Atmospheric pressure (N/m ²)
P_1, P_r, P_n	Pressure at the 1st, r th, and n th inlet (N/m ²)
P_s, \bar{P}_s	Supply pressure (N/m ²), $\bar{P}_s = P_s/P_a$
t	Time (sec)
W	Load capacity (N)
x, y	Cartesian coordinates of air film
z, \bar{z}	Axial coordinate of bearing, $\bar{z} = z/(L/D)$
Λ	Bearing number, $\Lambda = 6\mu\omega/P_a(C/R)^2$
Ω	Whirl frequency of journal center about the equilibrium axis
Ψ	Circumferential angle between adjacent restrictions, $\Psi = 2\pi/n$
ϕ_o	Steady-state attitude angle
μ	Dynamic viscosity of air (Ns/m ²)
θ	Angular coordinate, $\theta = x/R$
θ_r	Circumferential position of the r th feeding hole
τ	Non-dimensional time, $\tau = \Omega t$
ω	Spindle speed (rad/s)
γ	Whirl ratio

1 Introduction

Recently, high-precision products are widely required with job-shop type production and small batch production in the fields of manufacturing and machining [1]. For this end, high-speed and high-precision air spindles are widely used for hard disk drives, dental drills, and machining polygon mirrors for laser scanners. This is because high-speed rotation with small heat generation is possible for air spindles due to the low viscosity. It also gives rise to a noise-free and smooth running

M. Akhondzadeh (✉)
Engineering Department, Islamic Azad University,
Ahvaz branch, Khuzestan, Iran
e-mail: m_akhondzadeh@iauhvaz.ac.ir

M. Vahdati
Mechanical Engineering Department,
K. N. Toosi University of Technology, Tehran, Iran

and does not emit sound and vibration of the system in the way high-speed ball bearings do.

Air spindle and drive systems are important parts of ultra-precision machines, because the spindle motion error will have a significant effect on the surface quality and accuracy of machined components. Spindles in ultra-precision machines have high motion accuracy and rotational speed [2, 3].

Different researches have been committed on the characteristics of air bearings and their effect on system performance. In 1985 Boffey et al. investigated air pocket depth variations on air bearing stiffness, load capacity, and flow rate [4]. In 2000, Stout and Barrans presented a study in a design of aerostatic bearings for application to nanometer resolution manufacturing machine systems [5]. In 2002, Chen and Lin have analyzed static behavior and dynamic stability of grooved rectangular aerostatic thrust bearings with X-shaped grooves [6]. In 2002, Chen et al. investigated an arc-type aerostatic bearing with axial straight and the circumference arc-type grooves [7].

In 2009, Chen et al. investigated the effect of air pockets on aerostatic rotor-bearing system stability [8]. They studied the effects of feed holes and their number and position on aerostatic spindle stability by using non-dimensional Reynolds equation which was derived from Navier–Stokes and continuity equations. In 2002, Fan and Ho from Taiwan and Mou from Arizona presented an aerostatic air bearing system with multiple micro-holes [9]. They have prototyped multiple micro-holes instead of porous-type air bearing. Using porous material or multiple micro-holes will help to having a constant pressure distribution in air gap. In 2003, Noguchi and Miyaguchi have proposed an evaluation method of radial accuracy for hydrostatic air spindles considering the radial movement of the rotating center [10].

In 2004, Park and Kim have studied analytically and experimentally the stability of spindle system using a new type of slot-restricted gas journal bearings [11]. In 2009, Hirayama

et al. have optimized the groove dimensions in herringbone-grooved journal bearings for improved repeatable run-out characteristics [12]. In 2009, Chen et al. have presented a comparison in stability of rotor-aerostatic bearing system compensated by orifices and inferences [13]. In this study, the influences of the number and the locations of air entries on the aerostatic bearing are also estimated. In 2010 Chen et al. theoretically and experimentally analyzed a compound restrictor circular gas bearing with three straight and arc shallow grooves machined on the bearing surface, along which the supplied gas flows and reported same results for air film thickness effects [14].

In 2011, Xuedong Chen et al. have been investigated numerically the flow field in aerostatic bearings and experimentally measured the vibration of the aerostatic bearing [15]. They have established a direct relationship between the gas vortices and nano vibration in aerostatic bearings.

In 2013, Akhondzadeh and Vahdati have investigated the effect of size and number of rectangular air pockets on air spindle vibrations [16]. In their research, air pockets with minimum number and size have shown minimum vibrations. In 2013, Akhondzadeh and Vahdati, also, investigated the effect of shape and depth of air pockets on air spindle vibrations in ultra-precision machining [17]. They expressed that the air spindle with a rectangle shape of air pocket at a low rotational speed has minimum vibrations. In 2013, Akhondzadeh and Vahdati investigated the effects of shape, depth, size, and number of air pockets on air spindle vibrations altogether and performed 243 experiments [18].

In previous researches, air pocket depth was constant, i.e., depth has a same value in all points of air pocket. In this study, the air pocket is considered with variable depths, i.e., depth varies in different points of air pocket. The experimental setup is the same with [16–18]. In this study, 18 experiments committed, and the design of experiment (DOE) method has been used for result analysis.

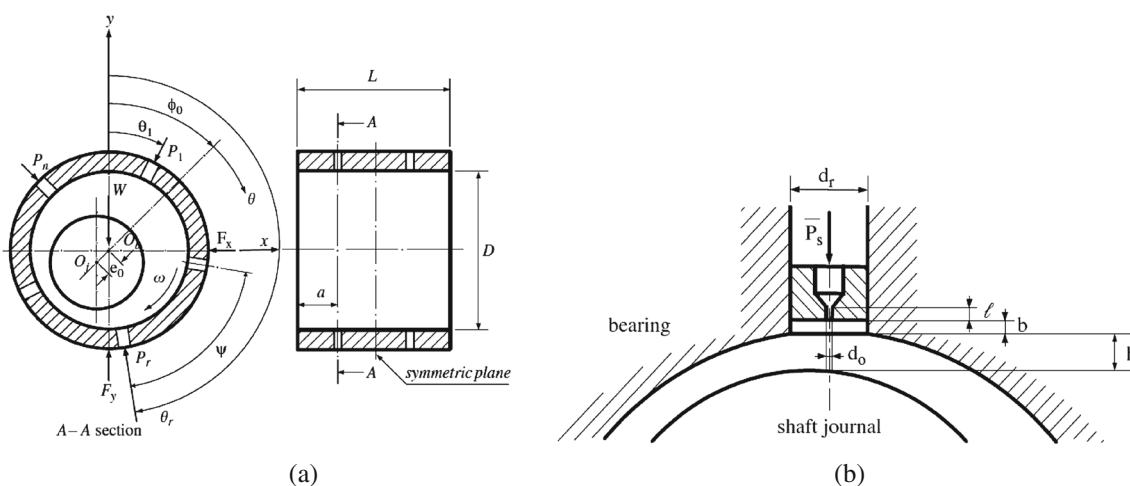


Fig. 1 Configurations of **a** an aerostatic bearing with double-array entries compensated by **b** orifice restriction

Table 1 The values selected for experiment parameters

Experiment parameters		
Value	Air pocket depth mode	Rotational speed (rpm)
1	Flat	1800
2	Conical	2556
3	Pyramidal	3600
4	Spherical (radius=25 mm)	
5	Spherical (radius=50 mm)	
6	Constant depth	

2 Air bearing equations

For an aerostatic journal bearing, as shown in Fig. 1a, air is supplied from an externally pressurized source and passes through entries with orifice pressure compensation as shown in Fig. 1b, which are located double-rows about asymmetric plane and evenly around the circumference of the bearing [19].

Assuming air at the bearing clearance as perfect gas which is compressible, isothermal, and laminar flow, the non-dimensional Reynolds equation could be derived from Navier–Stokes and continuity equations. In the two-dimensional Cartesian coordinate system, it may be shown as follows:


$$\frac{\partial}{\partial \theta} \left[\frac{1}{h^3} \frac{\partial P^2}{\partial \theta} \right] + \left(\frac{D}{L} \right)^2 \frac{\partial}{\partial z} \left[h^3 \frac{\partial P^2}{\partial z} \right] = 2\Lambda \frac{\partial}{\partial \theta} (Ph) + 4\gamma\Lambda \frac{\partial (Ph)}{\partial \tau} \quad (1)$$

where D and L are bearing diameter and length, P and h are non-dimensional pressure and thickness of film, y and z are angular and axial coordinates of bearing, respectively, t is non-dimensional time, L is bearing number, and g is whirl ratio.

3 Design of air spindles

Table 1 shows the values for each parameter used for investigation. The circular air pockets have selected for air pocket shape. Also, air pocket depth of equally 5 mm was selected. Size of air pockets has been designed in order to have a selected area shown in Table 2. The number for air pockets was selected as 3.

Table 2 The dimensions for variable depth pockets

Air pocket shape	Air pocket size (mm)
	$r = 11.3$

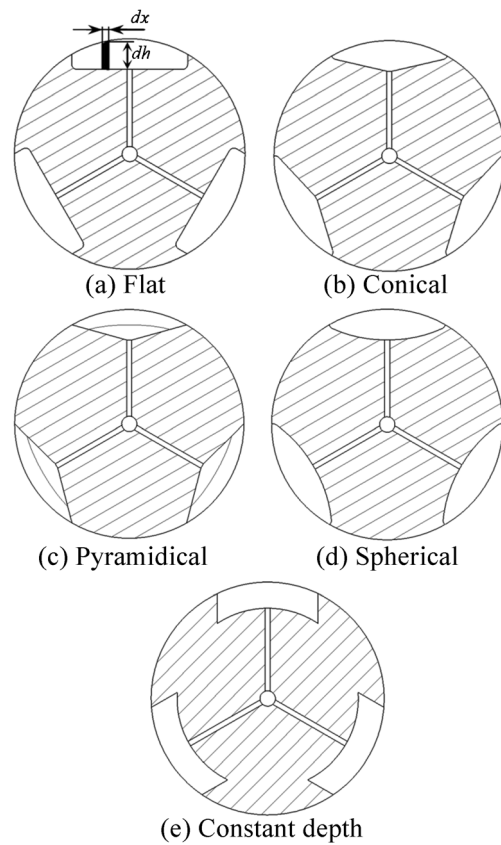


Fig. 2 Section view of air pockets

The section view of variable depth air pockets is showed in Fig. 2. As shown in Fig. 2a–d, air pocket depth varies with respect to a stator surface from feeding orifice to air pocket edge. The air pocket depth in Fig. 2e is constant, and the depth of air pockets has no variation in all points.

Stainless steel was chosen for rotor and stator material. Rotor has been considered externally which rotates about a stator. The air gap between a rotor and stator was selected as 25 μm.

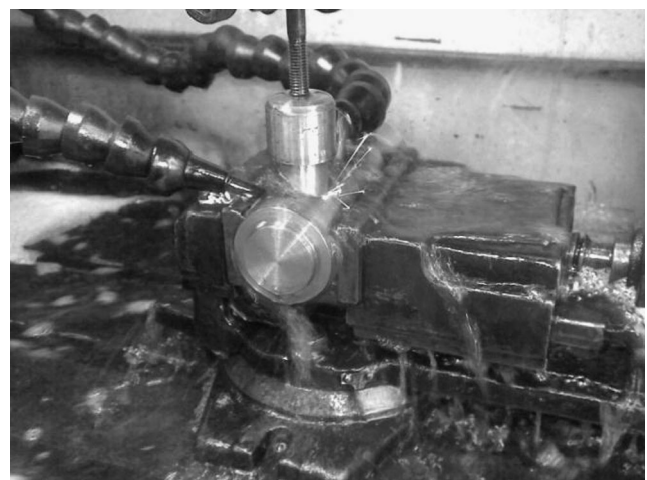


Fig. 3 Manufacturing of variable depth air pockets by EDM process

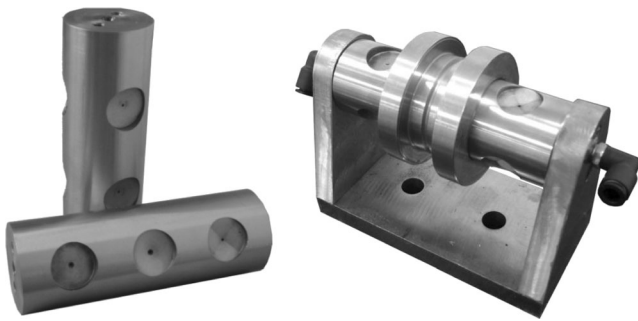


Fig. 4 Manufactured stators and a set of assembled spindle

For mounting air spindle on the lathe cross-slide, a base was designed and bolted on it. Air pockets on all stators were located at equal angular positions around a stator.

4 Manufacturing of air spindles

Various production processes were employed to manufacture the parts that were designed previously. The machining processes includes the following: facing and turning of stators, creation of variable depth air pockets electro-discharge machining (EDM), drilling, 1-mm feeding orifices drilling, holes threading, grinding of external surfaces of stators and internal surface of a rotor by cylindrical grind, and finishing of stators and rotor surfaces by sand.

Figure 3 shows the creation process of variable depth air pockets by EDM. Figure 4 shows manufactured stators and a set of manufactured stator and rotor.

5 Experimental setup

Figure 5 shows the experimental setup.

The test rig includes the following:

Lathe machine—for performing experiments on its cross-slide, which disassembled its compound slide rest and mounted

Fig. 5 Experimental setup

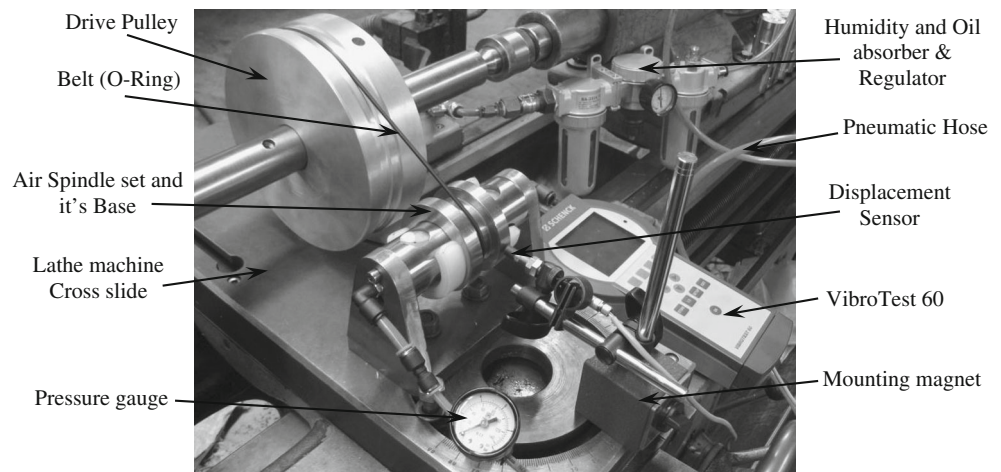


Fig. 6 The VibroTest 60 setups

test base on cross-slide. Air spindle and base—that were manufactured previously. Drive pulley—that transmits the lathe work holder rotational motion to rotor. O-ring—as belt that transmits rotational motion from drive pulley to a rotor.

Air compressor—for providing compressed air. Humidity and oil absorber—for absorbing water, oil, and other particles in compressed air duo to compressor working and preventing from entering air gap. Pressure regulator and Pressure gauge—for setting desirable air pressure value and assurance of air pressure on stator entrance, respectively. Air hose—for transmitting compressed air from compressor to air spindle.

Vibration measurement set—that contains VibroTest 60 for vibration measuring, displacement sensor IN-085 for vibration sensing, mounting magnet for sensor installation, and 1.5-mm thick feeler for setup of sensor with respect to a rotor surface.

The VibroTest 60 setups that must performed for vibrations measurement includes the following:

Sensor type—IN-085

Measurement amplitude—peak (p)

Measurement unit—micrometer (μm)

High and low pass frequencies—10–1,000 Hz

Table 3 The measured displacement values

Experiment parameters			
Test run	Air pocket depth mode	Rotational speed	Displacement (μm)
1	1	1	12.834
2	1	2	13.025
3	1	3	12.649
4	2	1	10.634
5	2	2	10.681
6	2	3	11.454
7	3	1	9.575
8	3	2	10.912
9	3	3	10.465
10	4	1	10.347
11	4	2	12.357
12	4	3	13.417
13	5	1	10.719
14	5	2	11.315
15	5	3	13.267
16	6	1	14.823
17	6	2	17.871
18	6	3	17.561

Vibration measurement was set on VibroTest 60. Mounting magnet was set for sensor installation. A 1.5-mm thick feeler was employed for set up of sensor with respect to the rotor surface.

High and low pass frequencies selected 10–1,000 Hz to prevent the impressibility of air spindle vibrations from vibrations likely induced by the lathe or the rotary pulley. Beside, as shown in Fig. 5, the displacement sensor has positioned on cross-slide, and vibrations induced by the lathe have been eliminated from vibration-measuring process.

Rotational speeds on lathe machine have been set on 500, 710, and 1,000 rpm and therefore by 1:3.6 ratios of pulleys, the experimental rotational speeds are 1,800, 2,556, and 3,600 rpm, respectively. Figure 6 shows the VibroTest 60 setups.

Table 4 The Analysis of variance of experiment results

Resource of variations	Sum of squares	Degree of freedom	Mean of squares	F0	P value
A	78.501	5	15.700	23.27	0.000
B	8.718	2	4.359	6.46	0.016
Error	6.746	10	0.675		
Total	93.965	17			

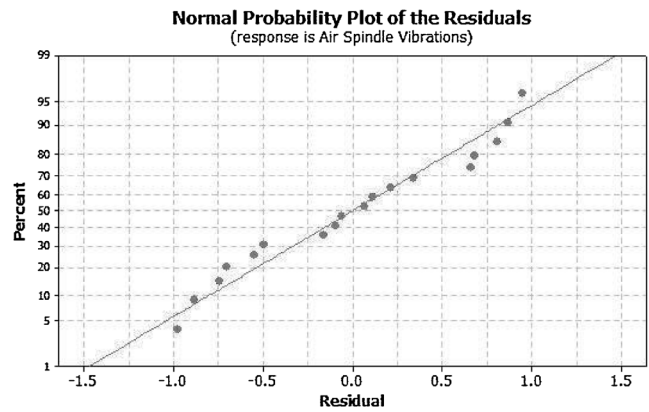


Fig. 7 The normal probability plot of the residuals for air spindle vibrations

6 Results and discussion

Measured displacement values are listed in Table 3. For analyzing the measured values, the design of experiments (DOE) method is employed. The analysis of variance (ANOVA) for these results is shown in Table 4.

According to ANOVA results, all studied parameters are significant in air spindle vibrations. In order to figure out the parameter levels in which air spindle vibration is minimized, the main effect and interaction plot of these parameters have been plotted.

The normal probability plot of the residuals for air spindle vibrations is shown in Fig. 7. Figures 8 and 9 show the plot of main effects in air pocket depth mode and rotor rotational speed, respectively.

From Fig. 7, the air spindle displacement values have a normal distribution. From Fig. 8, it seems that the air pockets with pyramidal depth mode have minimum vibrations. Also, constant depth air pockets show maximum air spindle vibrations. From Fig. 9, air spindles in the lowest rotational speed have a minimum vibration.

Figure 10 shows the interaction effect plots of air pocket depth mode and rotational speed on air spindle vibrations.

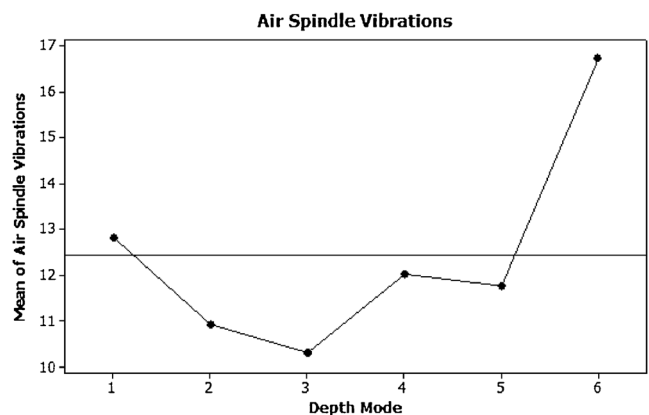


Fig. 8 The main effect of air pocket depth mode on air spindle vibrations

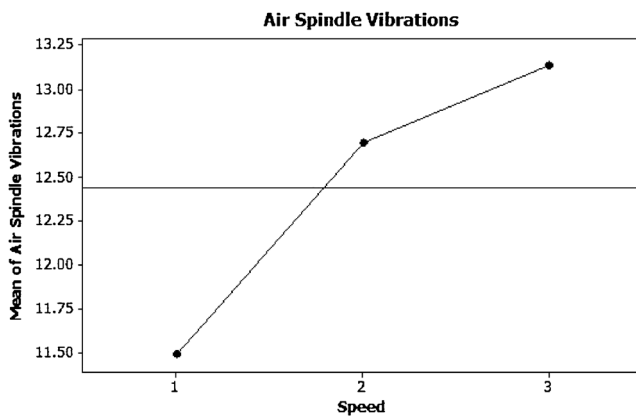


Fig. 9 The main effect of rotor rotational speed on air spindle vibrations

According to Fig. 10, spindle with pyramidal depth mode air pockets at 1,800 rpm rotational speed shows minimum vibrations.

According to results and effect plots, variable depth air pockets cause lower vibrations in air spindle. Maybe, piecemeal reduction in air pocket depth is a reason for the lower vibration in variable depth air pockets.

7 Conclusion

1. Air spindle vibration has a main effect on machined surface roughness. Air pocket geometry plays a main role in air spindle vibrations.
2. Air pockets with variable depths have been investigated in these experiments. It seems that variable depth air pockets provide a better pressure distribution in air gap.
3. From DOE, in air spindle vibrations and all studied parameters are significant.
4. Air spindles with pyramidal depth mode air pockets and at the lowest rotational speed have minimum vibrations.
5. In higher rotational speeds, also, the air spindles with pyramidal depth mode air pockets have minimum vibrations.

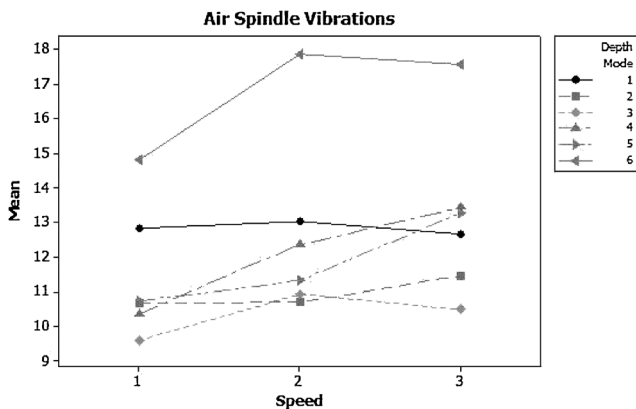


Fig. 10 The interaction effect plot of air pocket depth mode and rotational speed on air spindle vibrations

6. The air spindles with constant depth air pockets at highest rotational speed have a maximum displacement.

References

1. Weck M, Koch A (1993) Spindle-bearing systems for high-speed applications in machine tools. *Ann CIRP* 42:445–448
2. Venkatesh V. C. (2007) *Sudin Izman; "Precision Engineering"*; Tata McGraw-Hill Publishing Company Limited
3. Luo X (2005) Design of ultra precision machine tools with applications to manufacture of miniature and micro component. *J Mater Process Technol* 167:515–528
4. Boffey DA, Barrow AA, Deardent JK (1985) Experimental investigation into the performance of an aerostatic industrial thrust bearing. *Tribol Int* 18(3):165–168
5. Stout KJ, Barrans SM (2000) The design of aerostatic bearings for application to nanometer resolution manufacturing machine systems. *Tribol Int* 33:803–809
6. Chen MF, Lin YT (2002) Static behavior and dynamic stability analysis of grooved rectangular aerostatic thrust bearings by modified resistance network method. *Tribol Int* 35:329–338
7. Chen MF, Chen YP, Lin CD (2002) Research on the arc type aerostatic bearing for a PCB drilling station. *Tribol Int* 35:235–243
8. Chen CH, Yang DW, Kang Y, Hwang RM, Shyr SS (2009) Influence of orifices on stability of rotor-aerostatic bearing system. *Tribol Int* 42:1206–1219
9. Kuang-Chao F, Chi-Chung H, Jong-I M, Jong-I M (2002) Development of a multiple-microhole aerostatic air bearing system. *J Micromech Microeng* 12:636–643
10. Shoji N, Kazuo M (2003) An evaluation method of radial accuracy for hydrostatic air spindles considering radial movement of the rotating center. *Precis Eng* 27:395–400
11. Jung-Koo P, Kyung-Woong K (2004) Stability analyses and experiments of spindle system using new type of slot-restricted gas journal bearings. *Tribol Int* 37:451–462
12. Tomoko H, Naomi Y, Shingo S, Noriaki H, Takashi M, Hiroshi Y (2009) Optimization of groove dimensions in herringbone-grooved journal bearings for improved repeatable run-out characteristics. *Tribol Int* 42:675–681
13. Cheng-Hsien C, Ding-Wen Y, Yuan K, Ren-Ming H, Shyh-Shyong S (2009) Influence of orifices on stability of rotor-aerostatic bearing system. *Tribol Int* 42:1206–1219
14. Chen MF, Huang WL, Chen YP (2010) Design of the aerostatic linear guideway with a passive disk-spring compensator for PCB drilling machine". *Tribol Int* 43:395–403
15. Chen X, Chen H, Luo X, Ye Y, Hu Y, Xu J (2011) Air vortices and nano-vibration of aerostatic bearings. *Tribol Lett* 42(2): 179–183
16. Akhondzadeh M, Vahdati M (2013) Experimental investigation on effect of number and size of rectangular air pockets on air spindle vibrations in nanomachining. *Proc IMechE Part B: J Eng Manuf* 227(2):281–285
17. Akhondzadeh M, Vahdati M (2013) An experiment on the shape and depth of air pocket on air spindle vibrations in ultra precision machine tools. *Proc IMechE Part B: J Eng Manuf* 227(4): 616–620
18. Akhondzadeh M, Vahdati M (2014) Air pocket effects on air spindle vibrations in nanomachining". *Proc IMechE Part B: J Eng Manuf* 228(3):328–336
19. Cheng-Hsien H, Tsai T-H, Yang D-W, Kang Y, Chen J-H (2010) The comparison in stability of rotor-aerostatic bearing system compensated by orifices and inferences". *Tribol Int* 43:1360–1373